Non-rigid Volume Registration of Medical Images*

Vassili A. Kovalev[1] and Maria Petrou[2]

[1] Institute of Mathematics, Belarus Academy of Sciences, Gomel, Belarus
[2] School of Electronic Engineering, Information Technology and Mathematics, University of Surrey, Guildford, United Kingdom

This paper presents a global optimisation method for the registration of 3D medical images. A novel cost function is defined and it is optimised with the help of local non-linear elastic deformations. The terms of the cost function may be used as measurements of the degree of deformation, necessary to bring two images in registration, and also as quantifiers of the evolution of various pathologies.

1. Introduction

Registration of 3D volume medical data is important for two reasons. First, it allows the registration of images that refer to different individuals with the same reference image, for example the human atlas. If the reference image is already labelled and annotated, then the image under consideration is automatically labelled and annotated too (eg Christensen et al (1994) and Cuisenaire et al (1996)). Second, 3D registration of a succession of images that refer to the same individual may allow the monitoring of growth of various pathological lesions and the quantification of that growth as a function of time for regulating treatment, the co-registration of images of different modalities for improved diagnosis, etc.

For the above reasons, 3D volume registration has attracted a lot of attention in the recent years. For a review on these methods see Maurer and Fitzpatrick (1993). One characteristic of some medical tomographic images is the anisotropic resolution along the three axes directions. Thus, a volume medical image is often considered as a collection of 2D slices with spacing between them much larger than the size of pixels on each slice. This, plus the enormous amount of literature on the subject of rigid and non-rigid registration of 2D images, has led to the approaches of registration of volume data on the slice-by-slice basis (eg Kim et al (1997)). Such approaches, however, are not benefited by the correlation which obviously exists between successive slices. Methods specifically developed for 3D registration, take into consideration this correlation and thus belong to the class of genuine 3D methods. Most of these methods fall into two categories: surface registration and volume registration. Surface registration methods may rely on the identification of some landmarks on the surfaces to be registered, used to aid the process of registration (eg Thompson and Toga (1996)) or on the calculation of moments. In this group of methods one should perhaps also include the methods that attempt to perform segmentation and matching in one go, by using, for example, flexible shape objects identified within the image with the help of active "bubbles" (as opposed to active "snakes" in 2D) (Tek and Kimia (1997)). Once the surfaces have been registered, the registration of the volumes they enclose is implicitly also defined. This, however, means that volume characteristics are ignored by not being explicitly included in the process. Volume based methods tend to be computationally very slow, but they register volumes with volumes, making explicit use of all the data. Several of these methods are solid body registrations (Friston et al (1995), Woods

* The authors are grateful to the Royal Society for the grant that made this work possible.

et al (1993), Kiebel et al (1997)) assuming that non-linear inhomogeneous and anisotropic deformations are of negligible size. The most advanced methods are non-rigid volume matching approaches (Christensen et al (1994)). These methods effectively calculate the Maximum A Posteriori (MAP) solution of the problem, i.e. they find the most probable deformation that could lead from one volume to the other, given the data and a material model imposed on them. They are similar to the optic flow estimation methods where each voxel is assigned a vector indicating the way its position changes from one image to the next. The optimal configuration of assigned vectors is identified with the help of stochastic global optimisation of the cost function that incorporates smoothness constraints for the assigned vectors and a faithfulness to the data term. These methods produce excellent results, but they tend to be impossibly slow. The more powerful a method is, the more computationally expensive it becomes. Even rigid body methods are quite slow and attempts have been made to accelerate them (Alpert et al (1996)).

This is even more so for the 3D non-linear approaches involving stochastic optimisation. These methods require parallel implementation on special computer architectures if they are to be used at all (Christensen et al (1996)).

Because of this, several compromise approaches have been proposed. These approaches do not guarantee finding the optimal solution in the MAP sense. They simply find good sub-optimal solutions. Several of them use correlation methods and, for example, they identify the flow vector of a voxel guided by a local block correlation estimate (Richardson and Bury (1996), Gee and Haynor (1996)). However, in all cases, even if the optimisation approach used is guaranteed to find the optimal solution, the solution will be only as good as the model adopted allows it to be. For example, if surface processes (corresponding to "line processes" in 2D) are not incorporated in the cost function, the boundary surfaces between different components in the images may be blurred. If the smoothness constraint imposed corresponds to that of the thin plate in 2D, as opposed to that of the membrane, a different solution may be found.

The method we propose here differs from all the above methods in the following ways:

- The global constraint imposed by it is not one of arbitrarily defined local smoothness. It rather requires that the overall distortion one of the objects suffers to fit the other is the minimum possible, no matter how inhomogeneous it might be. This allows the distortion to be as un-smooth as it is locally required, so that it may model, for example, more accurately the growth of a localised tumour.

- It updates the displacement vectors of all the voxels in one go, rather than updating the displacement vector of one or a few voxels at a time. This allows faster convergence, and at the same time it implicitly incorporates a smoothness constraint which imitates the properties of an elastic medium better than thin plate or membrane models do.

In section 2 we shall formulate the problem and define our notation. In section 3 we shall describe the preprocessing stage of our approach, that results in the gross registration of the images, and in section 4 we shall describe the refinement of this gross registration using local non-rigid deformations and global optimisation. We present our experimental results in section 5 and our conclusions in section 6.

2. Problem Formulation

We assume that we have two images, I_1 and I_2. We shall use image I_1 as the reference image while image I_2 has to be deformed to come into registration with I_1. First, we preprocess the images, in the way described in the next section, so that the coordinate systems with respect to which the positions of the voxels in the two images are referred, are in registration. Thus, a voxel i at location (x_i, y_i, z_i), is supposed to have grey value p_i^1 in the first image and p_i^2 in the second image. To register the two images, we create a sequence of gradually deformed images, starting from I_2, and denoted by I_3, I_4,.... The grey value, p_i^l, of each voxel i in I_l has to be chosen with the help of image I_{l-1} so that the similarity of image I_l with I_1 is greater than the similarity of image I_{l-1} with I_1.

We need, therefore, to establish two things:

- A way that allows the generation of image I_l from image I_{l-1}.
- A measure of similarity between two images.

When the measure of similarity between the last image in the sequence created and image I_1 has not shown any significant improvement for the last few images in the sequence, the process may be terminated.

3. Pre-registration

We assume that the objects that are to be registered have been segmented and the voxels that belong to them in each image are suitably labelled. This is not necessary, as the algorithm can register whole images, but as we demonstrate it on the registration of brain data, we assume that the brain voxels for registration have been identified. First, we bring the two images in rough registration, using rigid body translation and scaling. We distinguish two types of scaling: that which is necessary because of the different sampling rates used to create different images, and the scaling that is required so that the objects depicted in the two images are made to have roughly the same size. The images are usually represented in terms of triplets of integer pixel indices, with the sampling rate given as extra information. To make sure that distances in both images are measured in the same units, we convert all pixel locations into real numbers, multiplying each pixel index with the corresponding inter-voxel distance in *mm*. Next, the centre of gravity of each of the two objects to be registered is found, and the two coordinate systems are shifted relative to each other, so that the two co-ordinate systems are in complete registration with each other and the two objects have coincident centres of gravity, the common origin of the coordinate systems. We do not use any rotation, although that could be also incorporated in this preliminary stage, because it was not deemed necessary: the brain images we had for our experimentation were not significantly rotated with respect to each other. The centre of gravity is calculated from the binary (labelled) images, and it is adequate for calculating the initial coarse registration of more or less convex objects. For irregularly shaped objects like ventricles in the brain, this simple approach may not be adequate.

Once the locations of the voxels in the two images refer to axes with the same origin and with identical units, we have to deal with the problem of different size of the objects that are to be registered. To deal with this, one of the two images is stretched isotropically, away from (or towards) the common centre of gravity of the two objects: Every voxel i at distance d_i from the origin is moved to a new location along the same radial direction from the origin and at distance from it td_i, where t is a stretching parameter. Then the image is re-sampled so that the locations for which we have values are the same for both images. This implies some interpolation, and for the sake of simplicity in computation we use the nearest neighbour interpolation rule. Then we calculate the correlation coefficient between the two images, defined as:

$$R_t(I_1, I_2) = \frac{\sum_{i \in \mathcal{A}_{12}^t} \left(p_i^1 - \bar{p}^1\right)\left(p_i^2 - \bar{p}^2\right)}{\sqrt{\sum_{i \in \mathcal{A}_{12}^t} \left(p_i^1 - \bar{p}^1\right)^2 \sum_{j \in \mathcal{A}_{12}^t} \left(p_j^2 - \bar{p}^2\right)^2}} \quad (1)$$

where $\mathcal{A}_{12}^t$ represents the *union* set of the voxels of the two objects, $\bar{p}^1$ is the mean grey value of the object in the first image, and $\bar{p}^2$ is the grey value of the object in the second image.

This is repeated for several values of t, both smaller than 1 (implying shrinkage) and larger than 1 (implying expansion) of the scaled image. The correlation coefficient is plotted as function of t and the value of t that maximises it is selected, as the necessary scaling parameter, for registering the two objects preliminarily. $R_t(I_1, I_2)$ as a function of t is a well behaved function, usually having a single, well defined maximum, if the label used for the background voxels is 0. (The background voxels enter the calculation through the parts which belong to the object in one image but they are not covered by the object in the other image, since we are computing the correlation over the union of the sets of voxels of the two objects.) This allows us to sample the range of values t may take quite grossly originally, and then to restrict the range and re-sample it more finely so that a more accurate value of t is identified. A typical range of values of t explored is $[0.75, 1.25]$.

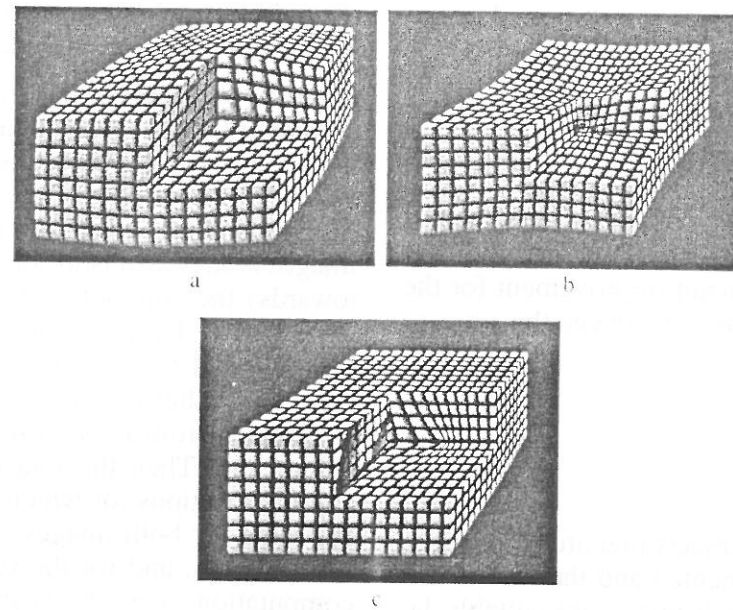

Fig. 1. Effects of the three deformation operators used on a regular $128 \times 128 \times 64$ lattice: (a) Exponential growth (b) Exponential shrinkage (c) Exponential shift.

The gross registration of the two objects obtained in this way is subsequently refined by the proposed non-rigid registration method described in the next section.

4. The Proposed Global Optimisation Approach

In order to distort image I_{l-1} we adopt the following process: We define three deformation operators: Exponential growth, Exponential shrinkage and Exponential translation. At each iteration step we choose at random one of the three operators to apply to the grid of the image. If the exponential growth (shrinkage) operator is chosen, then an arbitrary voxel i is chosen at random, and all other voxels k are shifted radially away (towards) voxel i by distance d_k given by equation $d_k = re^{-gd_{ik}}$ where r and g are some parameters and d_{ik} is the distance of voxel k from i. The values of the parameters are chosen so that the spatial order of the voxels is preserved. If the translation operator is chosen we proceed to choose at random a pair of voxel positions (x_i, y_i, z_i) and (x_j, y_j, z_j), within a certain distance d from each other. All the remaining voxels of image I_{l-1} will shift in location according to the following law: A voxel k will move in the direction of the vector defined from i to j, and by a distance given by $d_k = d_{ij}e^{-sd_{ik}}$, where d_{ij} is the distance between j and i, d_{ik} is the distance between k and i, and s is the "springiness" parameter that controls the severity of distortion. Figure 1 demonstrates the effect on the lattice of the image of each distortion operator used.

The grey values at the integer positions of the image grid are calculated using the nearest neighbour interpolation rule. These interpolated values are only used for the comparison of the distorted image with the target image. Once this comparison is made, these values are discarded, and the next image in the sequence is formed from the non-integer positions of voxels in grid I_l.

The deformed grid is accepted as the next grid I_l in the sequence, provided that it reduces the cost function of the quality of registration with image I_1. If it does not, grid I_l in the sequence is chosen to be the same as grid I_{l-1}.

The cost function expressing the quality of registration between images I_1 and I_l is defined as follows:

$$U = \alpha U_1 + \beta U_2 + \gamma U_3. \qquad (2)$$

In this expression, α, β and γ are parameters controlling the relative importance of each term. The three terms combined are the following:

$$U_1 \equiv 1 - R(I_1, I_l), \qquad (3)$$

where $R(I_1, I_l)$ is the correlation coefficient between the two images, defined in a similar way as in equation 1, except that now only the *overlapping* parts of the objects to be matched are used instead of their union. We denote the set of common voxels between the objects in images I_1 and I_l by $B_{1,l}$.

The next term expresses the desire for image I_l to be distorted as little as possible to fit image I_1. It is a purely geometric term that does not involve any grey values:

$$U_2 \equiv \frac{1}{N_{1,l}} \sum_{k \in B_{1,l}} \Big(|x_{k+1} - x_k - d_{xx}| + |y_{k+1} - y_k - d_{xy}| + |z_{k+1} - z_k - d_{xz}| + |x_{k+N_x} - x_k - d_{yx}| + |y_{k+N_x} - y_k - d_{yy}| + |z_{k+N_x} - z_k - d_{yz}| + |x_{k+N_x N_y} - x_k - d_{zx}| + |y_{k+N_x N_y} - y_k - d_{zy}| + |z_{k+N_x N_y} - z_k - d_{zz}| \Big)$$

where N_x and N_y is the size of the image along the x and the y axes respectively, and $N_{1,l}$ is the number of voxels in $B_{1,l}$. $d_{\alpha\beta}$ is the difference in coordinate values along the β axis, of two neighbouring voxels "aligned" along the α axis. In a regular grid, $d_{xx} = d_{yy} = d_{zz} = 1$ and $d_{xy} = d_{xz} = d_{yx} = d_{yz} = d_{zx} = d_{zy} = 0$. Here, we have values different from these due to the scaling we had to do to account for the anisotropic sampling of the images and the different object size. Note that k scans the image in a raster fashion, along the x axis on each successive slice corresponding to fixed z. More explicitly, the meaning of the first term, for example, in this function, is the following: x_{k+1} and x_k are the coordinate positions along the x axis of the two neighbouring voxels with indices $k+1$ and k respectively. At the beginning of the iterative process, the difference between these two coordinates is d_{xx}, since these voxels are next to each other along the x axis. After an iteration takes place, the two voxels may shift with respect to each other, so their distance along the x axis may have changed. The difference between this distance and the original value d_{xx}, expresses the distortion of the rigid grid. In a similar way, term $|x_{k+N_x} - x_k - d_{yx}|$ expresses the distortion of the grid away from the rigid one, due to the shifting in relative position of two neighbouring voxels along the y axis (indices $k + N_x$ and k identify neighbouring voxels along the y axis in a raster indexing format).

Finally, the third term of the cost function expresses the desire for maximum overlap between images I_1 and I_l:

$$U_3 \equiv 1 - \frac{N_{1,l}}{N} \tag{4}$$

where N is the maximum number of voxels in an image.

5. Experimentation

The preregistration of the images used in the experiments described below was done with isotropic stretching parameter t in the range $[0.9, 1.1]$. The search for the right value of t was conducted with step 0.33 of the size of a voxel.

Parameter r appearing in the exponential growth (shrinkage) operator was fixed for all experiments to $r = 1$. The value of the growth/shrinkage parameter g was chosen from a uniform distribution in the range $[0.1, 6]$, while parameters d and s for the exponential translation were chosen from the uniform distributions $[0.2, 6]$ and $[2, 5]$ respectively. Note that these values are in *mm*. After some trial and error the cost function parameters were fixed to $\alpha = 0.9$, $\beta = 0.005$ and $\gamma = 0.095$.

Figure 2 shows typical slices from two SPECT images of an AIDS patient. The brain component from the first image was registered with the brain component from the second image taken 8 months later from the same patient, after therapy with AZT. We also show the 3D "flow" vectors that indicate the deformation pattern of one slice.

Figure 3 presents two typical slices from two 3D MRI (T2) images of a patient with cavernous hemangioma in the hemisphere depicted on the left. The two images are taken with 4 months difference. From each image we extracted two volumes of interest (VOI), as marked on the figure, and in each volume the brain component was isolated manually. Our method was used to register the brain components (*not* the whole images) from the first image with their corresponding counterparts in the second image. Figure 4 shows how a typical slice from VOI1 in image 3a was deformed as a result of

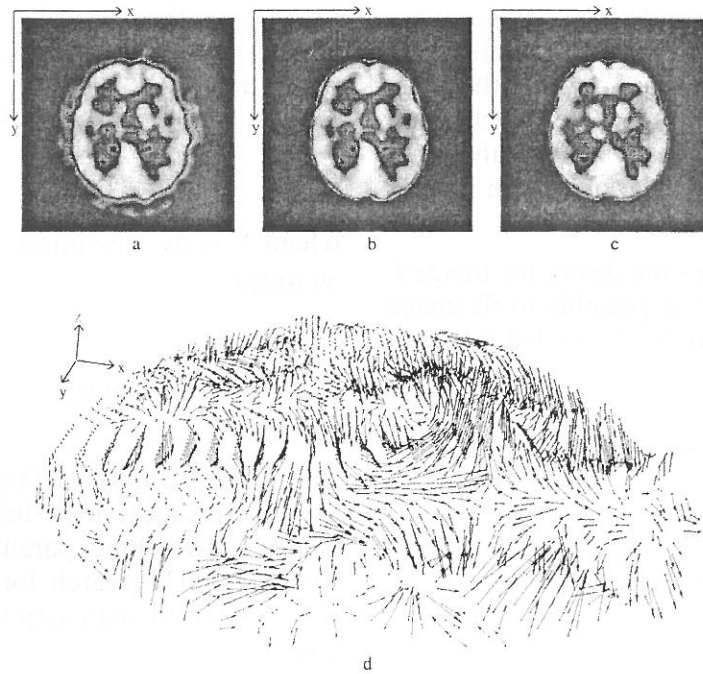

Fig. 2. Two original slices (b) and (c) of two 3D SPECT images of the brain of an AIDS patient taken with 8 months time difference, and the deformation field of the voxels of a slice (shown in 3D) when the two images are matched. In (a) we show the whole head image slice, before the segmentation of the brain.

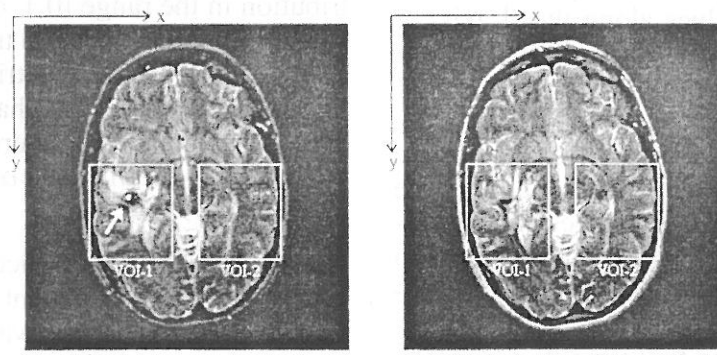

Fig. 3. Two corresponding original slices of two images from a patient with cavernous hemangioma taken 4 months apart. The rectangles mark the volumes of interest (VOI) that we match. Note that we use only the brain component present inside each 3D VOI.

the 3D registration of the VOI1 sub-images, and how little deformation the corresponding slice from VOI2 suffered as a result of the 3D registration of the VOI2 sub-images.

Figure 5 shows how the various components of the cost function change from one iteration step to the next for the two matchings performed. From this figure, it can be seen that the value of the deformity component, for example, can be used to quantify the degree of deformation due to the evolution of the pathological lesion (the value of the deformity converges to $U_2 = 0.760$ for VOI1 and to $U_2 = 0.316$ for VOI2). Notice that although we run 200,000 iterations, there is very little change in the values of the cost function after about 75,000 iterations. This number can be further reduced if the deformation operators are not applied entirely blindly. For example, figure 6a shows the number of times each of the three operators was used for an accepted deformation, at various stages of the registration of sub-images VOI1. To produce this graph, the total number of iterations used was divided into 30 bins of 6667 successive iterations each. The frequency of acceptance of each operator

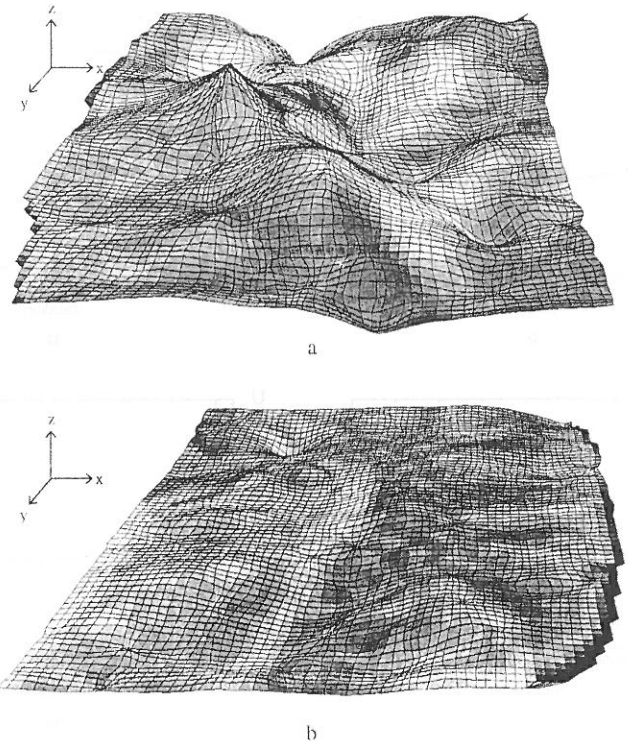

Fig. 4. (a) The deformed grid of a slice from VOI1 in figure 3a, after VOI1 of 3a was deformed to match VOI1 of 3b. (b) The deformed grid of a slice from VOI2 in figure 3a, after VOI2 of 3a was deformed to match VOI2 of 3b.

during the iterations that belong to the same bin was calculated and plotted. Note that these frequencies do not add up to 1 because there are many iteration steps when the deformation is not accepted and the image is not modified. It can be seen immediately that the exponential translation operator stopped being relevant after roughly the first 7,000 iterations. In the remaining 190,000 iteration steps it was picked up, tried, but the change it implied was not accepted. Given that the operators were picked at random, roughly 33% of the time taken by these iteration step was wasted. In figure 6b we plot the histogram of the accepted values of the growth/shrinkage parameter g. Again, it can be seen that, although all values in the range $[0.1, 6]$ were uniformly tried, the really relevant values were in the much smaller range of $[0.1, 2.5]$. It appears then that one can gain in efficiency by having a trial run of the registration process first, consisting of say 5,000 iterations, from which the acceptable range of parameters can be determined, as well as the relevance of the various operators. Once this has been established, the full registration can take place, with the parameters and operators chosen more effectively. The efficiency of a single run can be measured as the ratio of the number of iterations during which an operator was applied and its outcome was accepted, over the total number of iterations used. We repeated the experiment of matching sub-images VOI1 with an efficiency drive based on the use of the knowledge gained from a trial run. The efficiency of the run increased from 0.119 to 0.298. Figure 7 shows the cost function obtained from the efficient run, plotted with the cost function of the blind original run, as a function of the iteration step.

The algorithm requires 44 additions/subtractions per voxel, 14 multiplications/divisions, 1 exponential operation and 1 square root. In a Pentium 133 MHz PC machine it takes 1.88 secs per iteration on a 100,000 voxel object. In this time we also include the time to convert the numbers from the 4 bytes with which they are stored to save memory, to 8 bytes which are needed for performing the calculations. Typically about 50,000 iterations were needed for two volumes to be registered. This means that registration of two volumes using our PC took several hours. However, on a 0.8 GigaFLOPS machine, on which other flexible volume registration methods are reputed to require 9 hours,

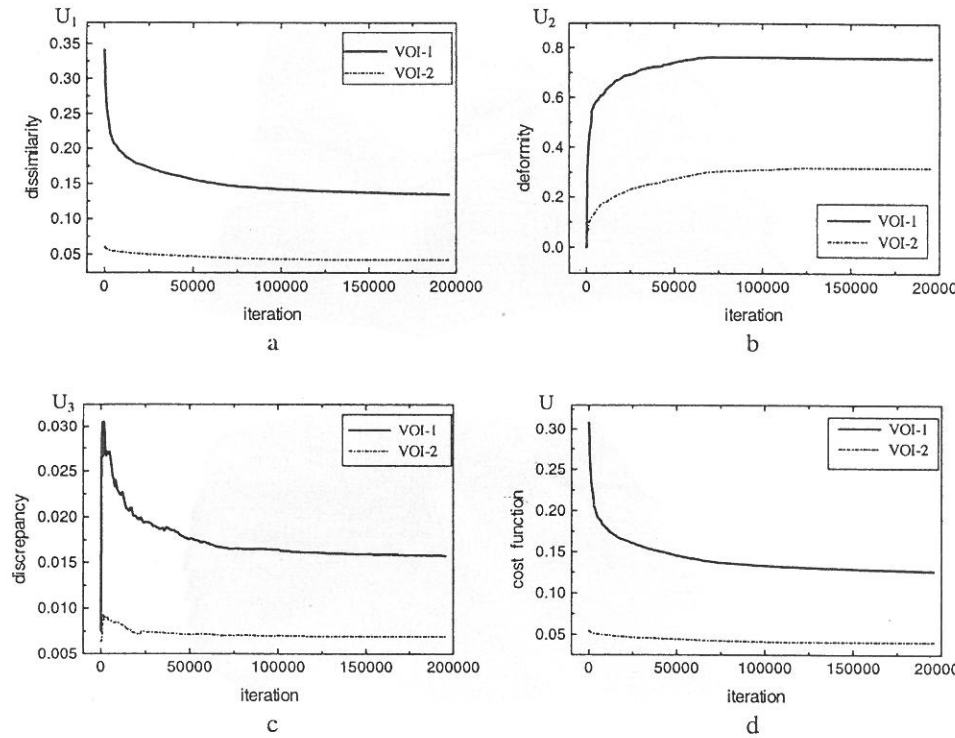

Fig. 5. The dissimilarity U_1 (in (a)), the deformation U_2 (in (b)), and the discrepancy U_3 (in (c)) terms of the cost function, and the cost function itself (in (d)) as functions of the iteration step of the matching procedure for the two volumes of interest (continuous line: VOI1 with pathology; dashed line: VOI2 with no obvious disturbance).

the proposed method would need only minutes (Christensen et al (1994), Thompson and Toga (1996)).

6. Conclusions

We have presented a method for flexible volume registration of medical 3D images. The method is based on the global optimisation of a cost function that allows incorporation of various constraints, measurements and items of prior knowledge concerning the problem, and the use of three types of non-linear exponential models of distortion. As such, it is a purely data and geometry driven method, with no reference to the underlying physical processes that take place which may or may not always be well understood. Our algorithm performs deterministic optimisation which accumulates the effect of stochastically chosen global non-linear deformations. Because of this the algorithm is considerably faster than stochastic optimisation algorithms: it may take minutes for a task that may require hours to be completed by a stochastic method. Of course, there is a penalty to be paid for not using a stochastic optimisation approach: there is no guarantee that the algorithm will converge to the global optimum. The solution reached may be a local minimum of the cost function. This is the case with all deterministic optimisation approaches, and even with stochastic ones when the strict slow cooling schedule necessary for convergence is not adhered to.

We showed that careful choice of the parameters and the operators used may lead to significant gains in efficiency. It is not possible to give here recipes on these choices. How efficiently a matching is performed depends very much on the type of images to be matched. Smooth images, which match well, can be matched much faster than severely deformed images. For example, the registration of sub-images VOI1 of figure 3, that contain the tumour, took much longer than the registration of sub-image VOI2, for the same parameter values.

Our method allows the mapping of *any* volume onto any other. For some researchers this may be considered as a drawback of the approach. However, as long as the topology is the same, it is true that any topology preserving algorithm

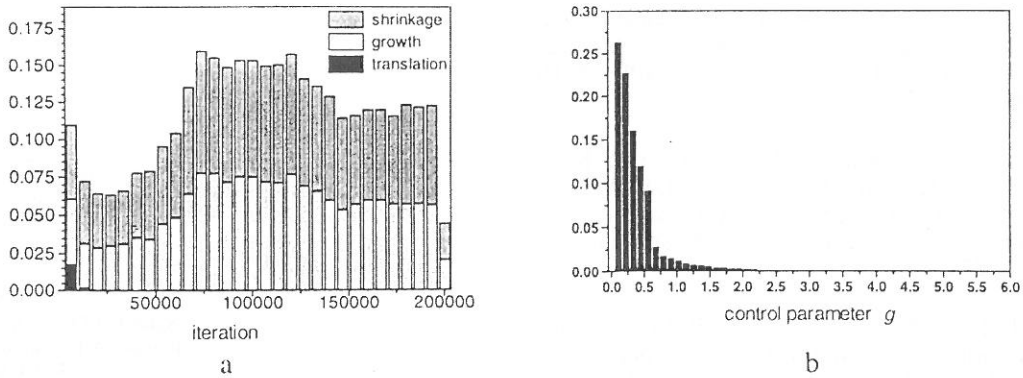

Fig. 6. (a) Frequency of acceptance of the deformations caused by the three operators as a function of the registration stage. (b) Frequency of occurrence of acceptable values of parameter g.

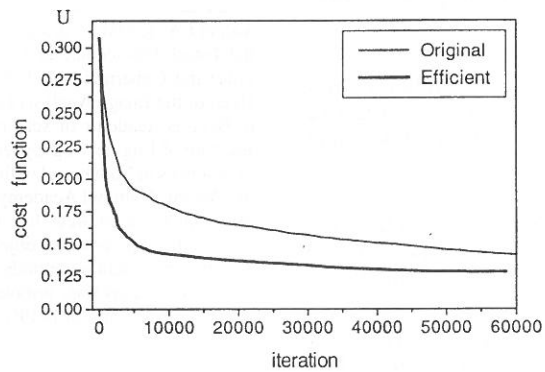

Fig. 7. The cost function of matching VOI1 with and without efficiency drive.

must have this property. Our algorithm is topology preserving, because the sequence of voxels is not changed when an exponential distortions is imposed. This does not mean, however, that our algorithm is appropriate only for small size deformations. Larger deformations are created as the accumulations of several small, topology preserving ones. On the other hand, since it is a correlation-based method, it is not suitable for the registration of volume raw data of different modalities. The method can be used for inter-modality registration, only if an appropriate transformation takes place first, to make the data of the two modalities compatible. This will involve careful analysis of the underlying physics of image formation. Whether a matching between two objects is acceptable or not, can be judged by the value of the deformation term of the cost function. This term expresses the geometric distortion an object has to suffer in order to match another one. Therefore, we propose it as a measure of the deformation caused by the growth of tumours, for example, and as a measure quantifying the similarity of the two objects in the first place.

7. References

N. M. ALPERT, D. BERDICHEVSKY, Z. LEVIN, E. D. MORRIS AND A. J. FISCHMAN, Improved methods for Image Registration. Neuroimage, 3 (1996), 10–18.

G. E. CHRISTENSEN, M. I. MILLER, M. W. VANNIER, Individualising Neuroanatomical Atlases using a massively parallel computer. IEEE Computer, 29 (1996), 32–38.

G. E. CHRISTENSEN, R. D. RABBIT AND M. J. MILLER 3D Brain Mapping using a Deformable Neuroanatomy. Physics in Medicine and Biology, 39 (1994), 609–618.

O. CUISENAIRE, J. P. THIRAN, B. MACQ, C. MICHEL, A. DEVOLTER AND F. MARQUES, Automatic registration of 3D MR Images with a computerised brain atlas. Medical Imaging 1996: Image Processing, SPIE 2710 (1996), 438–448.

K. J. FRISTON, J. ASHBURNER, C. D. FRITH, J–B. POLINE, J. D. HEATHER AND R. S. FRACKOWIAK, Spatial registration and normalisation of images. Human Brain Map, 2 (1995), 165–189.

J. C. GEE AND D. R. HAYNOR, Rapid coarse-to-fine matching using scale-specific priors. Medical Imaging 1996: Image Processing, SPIE 2710 (1996), 416–427.

S. J. KIEBEL, J. ASHBURNER, J-B. POLINE AND K. J. FRISTON, MRI and PET co-registration-A cross validation of Statistical parametric mapping and automated image registration. Neuroimage, 5 (1997), 271–279.

B. KIM, J. L. BOES, K. A. FREY AND C. R. MEYER, Mutual Information for Automated Un-warping of Rat Brain Autocardiographs. Neuroimage, 5 (1997), 31–40.

C. R. MAURER AND J. M. FITZPATRICK, A review of medical image registration. R J Maciunas ed, Interactive Image-guided Neurosurgery, (1993), 17–44.

D. B. RICHARDSON AND E. A. BURY, Correlative techniques for cross-modality medical image registration. Medical Imaging 1996: Image Processing, SPIE 2710 (1996), 368–375.

H. TEK AND B. B. KIMIA, Volumetric segmentation of Medical Images by 3D bubbles. Computer Vision and Image Understanding, 65 (1997), 246–258.

P. THOMPSON AND A. W. TOGA, A surface-based technique for warping 3D images of the brain. IEEE Transactions of Medical Imaging, 15 (1996), 402–417.

R. P. WOODS, J. C. MAZZIOTTA AND S. R. CHERRY MRI-PET registration with automated algorithm. Journal of Computer Assisted Tomography, 17 (1993), 536–546.

Received: July, 1997
Revised: May, 1998
Accepted: June, 1998

Contact address:

Vassili A. Kovalev
Institute of Mathematics
Belarus Academy of Sciences
Kirova St., 32-A
Gomel 246652
Belarus

Maria Petrou
School of Electronic Engineering
Information Technology and Maths
University of Surrey
Guildford GU2 5XH
United Kingdom
phone: +44 1483 259801
fax: +44 1483 259554
http://www.ee.surrey.ac.uk/Personal/M.Petrou/

VASSILI A. KOVALEV graduated in Applied Mathematics in 1978 from the Tomsk Polytechnic Institute, Russia and obtained his Ph.D. on Engineering Cybernetics in 1984 from the same institute. He has been Head of the Image Analysis Laboratory of the Institute of Mathematics of Belarus Academy of Sciences, in Gomel and he is currently with the Institute of Engineering Cybernetics of the Belarus National Academy of Sciences in Minsk, and with the Metal-Polymer Research Institute, of the Belarus National Academy of Sciences in Gomel. He has more than 80 publications in areas like texture feature extraction, segmentation, colour image processing, object recognition, 3D image processing and energy minimisation methods with applications in biomedical diagnostics, visual inspection, remote sensing, surface analysis, etc. He is a member of IEE and of IAPR.

MARIA PETROU received her BSc. in Physics in 1975 from the University of Thessaloniki, Greece, and her PhD. in Astronomy in 1981 from the University of Cambridge, United Kingdom. She has been working on computer vision since 1986, and has published more than 170 papers, more than 60 of which in refereed journals, on astronomy, low level vision, feature extraction, texture analysis, Markov random fields, probabilistic relaxation, colour, remote sensing, industrial inspection, medical signal processing, etc. She is Professor of image analysis at the School of Electronic Engineering, Information Technology and Mathematics of Surrey University, United Kingdom, and a member of the British Machine Vision Association, and of IEEE. She has served as an Associate Editor of IEEE Transactions on Image Processing and she is the Newsletter Editor of IAPR.